Biomaterials Science

ROYAL SOCIETY OF CHEMISTRY

PAPER

View Article Online
View Journal | View Issue

Cite this: *Biomater. Sci.*, 2022, **10**, 6486

Preparation and characterization of flexible furosemide-loaded biodegradable microneedles for intradermal drug delivery†

Arsalan Abu-Much, ‡[a,b] Raya Darawshi,‡[c] Hala Dawud,[c] Haytam Kasem[d] and Aiman Abu Ammar *[c]

Transdermal drug delivery systems are a useful and minimally invasive alternative to other drug administration routes. Biodegradable polymeric microneedles (MNs) are widely used in controlled–release drug delivery due to their tunable properties and ease of patient self-administration. Polylactic-*co*-glycolic acid (PLGA) is often used for sustained drug release owing to special intrinsic properties including biocompatibility and biodegradability, which offer excellent applicability in preparing MNs. Congestive heart failure (CHF) is characterized by fluid overload during acute exacerbation, necessitating frequent patient hospitalization for continuous intravenous (i.v.) diuretic therapy. In the present study, we incorporated furosemide (FUR) as a model drug into flexible PLGA MN skin patches for potential intradermal delivery to overcome the limitations associated with i.v. diuresis. The MNs were fabricated by a casting-mold technique and consisted of two main parts, PLGA needle tips loaded with varying concentrations of FUR and a flexible backing layer comprising sodium alginate and glycerol. MN formulations were characterized by SEM and exhibited a uniform pyramidal shape. The measured surface pH of all samples suggested that no skin irritation is expected upon application. High encapsulation efficiency was obtained for FUR-MN formulations in which a decrease was noted as the FUR/PLGA ratio decreased. Drug loading content ranged from 19.1 ± 1% to 28.9 ± 1.4%. Successful insertion of MNs into a Parafilm® skin simulant model suggested that MNs will easily penetrate the skin's outermost layer, the *stratum corneum*, and will permit intradermal delivery of FUR. The MNs were further characterized by analytical methods. Finally, the MNs exhibited an initial burst release followed by a sustained release of FUR. Self-administered FUR-MNs can open new avenues to overcome i.v. drip limitations and increase patient compliance.

Received 20th July 2022,
Accepted 22nd September 2022

DOI: 10.1039/d2bm01143c

rsc.li/biomaterials-science

1. Introduction

Transdermal drug delivery systems are well known for increasing the bioavailability of biopharmaceutical classification system class IV drugs, a class characterized by poor water solubility and low permeability. These minimally invasive systems constitute a suitable alternative to other drug administration routes such as intramuscular and intravenous (iv) administration.[1]

In recent decades biocompatible polymeric microneedles (MNs) have demonstrated an outstanding ability to encapsulate active compounds and deliver them across the skin in a painless and effective administration route for various applications. Polymeric MNs are widely used in controlled–release drug delivery as a result of their tunable properties and ease of patient self-administration.[2,3] Poly(lactic-*co*-glycolic acid) (PLGA) copolymer is often used for sustained drug release owing to its intrinsic properties including biocompatibility, biodegradability, and favorable mechanical performance.[4–8] Therefore, PLGA offers excellent applicability and is commonly used for preparing MNs.[3,9–12]

Congestive heart failure (CHF) has been recognized as a worldwide endemic, where numbers in the United States are expected to increase by 46% by 2030,[13] particularly as a result of population growth and aging.[14] It imposes a significant medical and economic burden characterized by a high 5-year mortality, reaching 53% from the moment of diagnosis. From a clinical perspective, fluid overload (*e.g.*, pulmonary conges-

[a]*Leviev Heart Center, Chaim Sheba Medical Center, Tel Hashomer, Ramat Gan, Israel*
[b]*Sackler School of Medicine, Tel Aviv University, Tel-Aviv, Israel*
[c]*Department of Pharmaceutical Engineering, Azrieli College of Engineering Jerusalem, 26 Yaakov Shreibom Street, Ramat Beit Hakerem, Jerusalem 9103501, Israel. E-mail: aimanab@jce.ac.il; Tel: +972-2-6591835*
[d]*Department of Mechanical Engineering, Azrieli College of Engineering Jerusalem, Jerusalem, Israel*

†Electronic supplementary information (ESI) available. See DOI: https://doi.org/10.1039/d2bm01143c

‡These authors contributed equally to this work.

tion, ascites, and lower limb edema) is among the hallmarks of acute exacerbation symptoms, necessitating frequent patient hospitalizations for diuretic therapy,[14] further contributing to substantial use of health care resources.[15]

Loop diuretics (*e.g.*, furosemide) are considered the mainstay of fluid overload treatment in CHF.[14] Intravenous furosemide (FUR) is twice as potent as oral administration due to higher drug bioavailability, particularly in the case of acute exacerbation, a state characterized by enhanced sodium retention,[16] The i.v. administration of FUR through syringe pump necessitates inpatient care, continuous monitoring, and peripheral i.v. catheter placement. This makes the strategy particularly inconvenient in addition to posing a significant risk from peripheral venous catheters associated with adverse events.[15,17] Therefore, novel therapeutic strategies for diuresis with different administration routes, such as subcutaneous (s.c.), have been developed to facilitate outpatient diuresis therapy and to minimize the in-hospital stay. For example, a novel buffered formulation of pH-neutral FUR (pH 7.4) was developed for s.c. infusion using a wearable patch pump. This showed comparable bioavailability and diuresis to the regular i.v. FUR bolus.[18] Another study has demonstrated consistent, effective, and safe diuresis using non-formulated FUR when administered s.c. *via* a syringe pump system.[19] Even so, this warrants the use of continuous infusions and skin canulation just like the i.v. route. Intradermal (i.d.) drug delivery has emerged as a better alternative to s.c. routes across different therapeutic agents, such as insulin[20] and monoclonal antibodies.[21] Data regarding the feasibly of i.d. delivery of FUR using MNs are scarce.

We aim to incorporate FUR as a model drug for self-applicable MN skin patches. They consist of FUR-loaded PLGA biodegradable needle tips and a flexible backing layer comprising sodium alginate and glycerol, for potential i.d. administration aimed at sustained diuresis in heart failure patients, thereby overcoming the limitations associated with continuous i.v. and s.c. drips.

2. Materials and methods

2.1. Materials

FUR (>98%) was purchased from Apollo Scientific Ltd (UK). PLGA-Purasorb PDLG 5010 (50 : 50) was donated by Corbion Purac (Gorinchem, The Netherlands). Silicone MPatch microneedle templates were purchased from Micropoint Technologies Pte Ltd (Pioneer Junction, Singapore) and were pyramidal in shape with a dimension of 10 × 10 needle array, 200 μm base, 500 μm height and 500 μm pitch. Phosphate buffer saline (PBS) was purchased from Hyclone Laboratories. Organic solvents and sodium alginate were obtained from Sigma-Aldrich (Rehovot, Israel).

2.2. Fabrication of FUR-loaded PLGA MNs

FUR-loaded PLGA MNs were prepared using a casting-mold technique[10] with modification as shown in Fig. 1. Briefly, 5% w/v solution of PLGA in chloroform containing varying concentrations of FUR was left to stir until a clear solution was obtained. For the two-step microneedle fabrication, 150 μL of FUR/PLGA solution was cast on polydimethylsiloxane (PDMS) microneedle molds and degassed in a vacuum for 2 min to fill mold cavities. Then, 100 μL of the back-layer solution comprising 2% w/v sodium alginate and 1% w/v glycerol in distilled water (DW) was added to the molds, and the templates were kept overnight in a desiccator. Finally, the MN patches were peeled off the mold and stored in a desiccator until future use (Fig. 1). Different MN formulations were prepared as shown in Table 1. In a typical preparation, appropriate amounts of PLGA and FUR were dissolved in chloroform. The weight ratio of FUR/PLGA in the solution was W_{FUR}/W_{PLGA} = 1/2 (FUR-MN2). The blank PLGA MNs (P-MN) were fabricated by the same procedure as FUR-loaded MNs without adding FUR at any stage of the preparation.

2.3. Morphological characterization of PLGA MNs

Morphological characterization of FUR-loaded MNs was carried out using an Environmental Scanning Electron Microscope (ESEM) (Quanta 200, FEI, Germany) to evaluate the surface morphology and dimensions of the MNs.

2.4. Folding endurance

The flexibility of the different PLGA MNs was assessed manually by folding each patch repeatedly at the same place using the thumb and forefinger until the patch broke or visible cracks appeared.[22] Three patches of each type were tested.

2.5. Determination of FUR encapsulation efficiency

The FUR-loaded MNs were dissolved in 1 mL acetone. Methanol was then added to precipitate the polymers, followed by vortex and centrifugation for 2 min at 2000 rpm. Afterwards, the supernatant containing the drug and organic solvents was transferred and evaporated. The resulting residue was subsequently dissolved in methanol, and FUR was quantitatively determined after suitable dilutions with the same solvent using a Biochrom UV-vis spectrophotometer at a wavelength of 275 nm. The concentrations of the calibration curve ranged from 0 to 20 μg mL^{-1} (Fig. S1†).

2.6. Surface pH

The surface pH of three prepared films of each formulation was determined after placement into glass tubes containing 10 ml of double distilled water for 2 h at room temperature. A combined glass electrode was located near the surface of the film, and pH measurements were performed after an equilibration time of 1 min[23]

2.7. Insertion capabilities of MN array in Parafilm®

PLGA MNs were manually pushed into 10 layers of Parafilm® for 30 s and observed under an optical microscope to study the mechanical insertion properties of the needles. The mechanical uniformity of PLGA MNs was estimated from the dimensions of 10 randomly selected pores created in the first layer

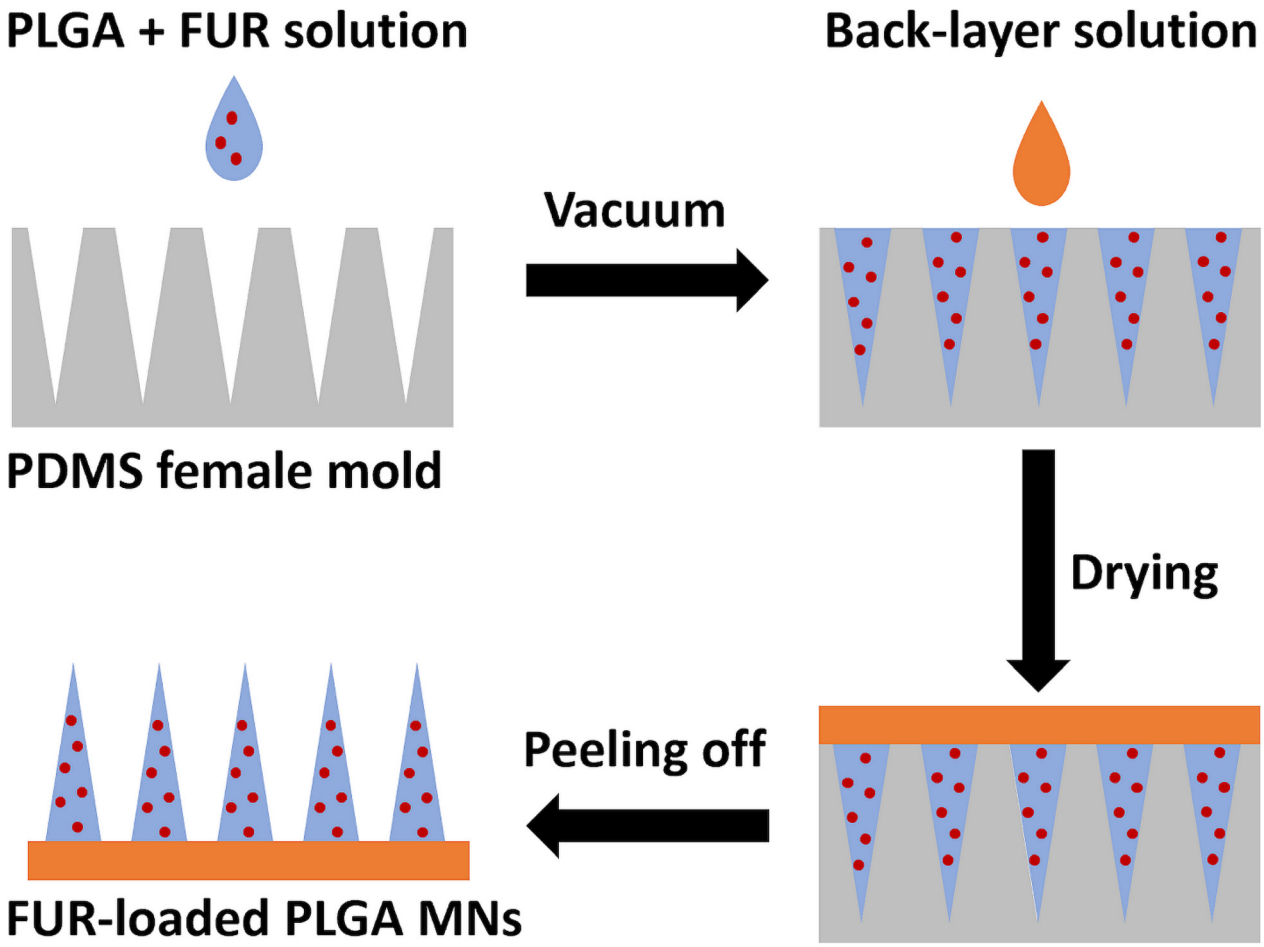

Fig. 1 Preparation scheme of FUR-loaded PLGA MNs using a polydimethylsiloxane (PDMS) microneedle mold.

Table 1 Composition of PLGA MNs

		Needle tip solution			
Condition designation	FUR : PLGA (% w/w)	FUR (mg)	PLGA (mg)	Chloroform (μL)	Back-layer solution
P-MN	—	—	7.5	150	2% Sodium alginate and 1% glycerol
FUR-MN2	1 : 2	3.75	7.5	150	
FUR-MN3	1 : 3	2.50	7.5	150	
FUR-MN4	1 : 4	1.87	7.5	150	

and the last (second) layer using ImageJ software (National Institute of Health, Bethesda, MD, USA).[24,25] The rate of change of the height (μm) of the MNs was calculated and plotted as the percentage of reduction in MN height.

2.8. Differential scanning calorimetry (DSC) measurements

DSC measurements were performed using a DSC 1 Star System equipped with Star Software (Mettler Toledo, Greifensee, Switzerland) and a DSC131 Evo (SETARAM Instrumentation, Caluire-etCuire, France). Weighed samples of 5–12 mg were placed into 100 μL aluminum crucibles, and the samples were scanned from −20 °C to 270 °C at a constant heating rate of 10 °C min^{-1} under a continuous flow of dry nitrogen.

2.9. Powder X-ray diffraction (PXRD)

PXRD measurements were performed using a D8 Advance diffractometer (Bruker AXS, Karlsruhe, Germany) with secondary Graphite monochromator, 2° Sollers slits and 0.2 mm receiving slit. Low-background quartz sample holders were carefully filled with the powder samples. XRD patterns within the range 2° to 75° 2θ were recorded at room temperature using CuKα radiation (λ = 1.5418 Å) with measurement con-

ditions: Tube voltage of 40 kV, tube current of 40 mA, step-scan mode with a step size of 0.02° 2θ and counting time of 1 s per step.

2.10. Attenuated total reflectance–Fourier transform infrared spectroscopy (ATR-FTIR) measurements

ATR-FTIR spectra were measured by a PerkinElmer Spectrum 100S spectrometer equipped with a universal ATR sampling accessory. The transmission spectra were recorded with a spectral range of 500–4000 cm^{-1}, against a background of air, using 4 scans with a resolution of 4 cm^{-1}.

2.11. *In vitro* drug release studies

Samples of FUR-MN2, FUR-MN3 and FUR-MN4 were placed into 10 mL of PBS (pH 7.4) and maintained at 37 °C in a rotary incubator (50 rpm). At predetermined intervals, 1 mL samples were withdrawn from the release medium and were replenished immediately with the same volume of fresh prewarmed PBS (37 °C) maintaining sink conditions throughout the experiment. The drug release experiment was performed at 37 °C to simulate the internal body temperature where the drug is presumably released from the microneedles.[26–28] FUR concentrations were determined following suitable dilution using a UV-vis spectrophotometer at a wavelength of 277 nm.[29] The concentrations of FUR calibration curve in PBS (pH 7.4) ranged from 0 to 30 μg mL^{-1} (Fig. S2†).

2.12. Evaluation of mechanical properties and *ex vivo* skin penetration of FUR-MN2

The mechanical strength of FUR-MN2 was determined using a customized tension/compression tester that was designed and built at the Tribology Laboratory, Azrieli College of Engineering Jerusalem.[30] The device is constructed on the basis of a one-pass vertical displacement consisting of driving and measuring units. In the present study, the lower counterface was made of a flat block of aluminum (Young's Modulus, $E \approx 69$ GPa) for the reference test and *ex vivo* chicken skin, obtained from a local slaughter house, for the penetration test.[26,31,32] The MN samples were glued to a hard support on a passive self-aligning system based on the principle of two free rotation axes to guarantee a full flat-on-flat contact between the mating surfaces. The self-aligning system is attached to a motorized linear actuator (A-LAR300APC-01, US) that can move to bring the mating surfaces in contact under a predefined constant loading velocity to reach the desired normal load and then, after a predefined waiting dwell time under the loaded state, the translation stage is withdrawn opposite to the normal direction. The measurement unit consists of an accurate load cell FUTEK (FSH00098, US) with a multifunctional data acquisition board Lab-PC-1200 (National Instruments Co., Austin, Texas, USA) and is processed using a LabVIEW software package (National Instruments Co., Austin, Texas, USA).

In this test, the MN arrays were pressed against a flat block of aluminum or chicken skin at a loading velocity of 0.2 mm s^{-1} until the desired normal force of 32 N is achieved (320 mN per needle), followed by 30 s waiting dwell time under the loaded state, then withdrawing the upper holder that holds the MNs samples in the opposite direction.[33] The load cell records the variation in the applied normal force as a function of the vertical displacement of the stage. The force *versus* displacement curves were generated for each test. Deformation of microneedles after the application of different compressive forces was examined by a stereomicroscope (Olympus SZ61) and the change in needle height following the application of the axial compression load was evaluated.

3. Results and discussion

The MNs consist of two main parts, FUR-loaded biodegradable needle tips made of PLGA and a flexible backing layer comprising sodium alginate and glycerol, which were fabricated through a casting-mold technique as illustrated in Fig. 2. The MNs were fabricated as a 10 × 10 array. The shapes of the manufactured polymer MN tips were quadrangular pyramids (Fig. 2A). The obtained MN patch was flexible to be easily folded without damaging the MN arrays (Fig. 2B) due to the use of glycerol as a plasticizer to impart flexibility to the backing layer.[34,35]

When characterized by SEM, all MN formulations had a quadrangular pyramidal shape and were uniformly distributed on the substrate (Fig. 3). P-MN, FUR-MN2, FUR-MN3 and FUR-MN4 were successfully fabricated with dimensions of 494.35–499.21 μm height and 196.62–199.31μm width of the base as depicted in Table 2. Additionally, the SEM images confirmed sharp tips of the MNs without any visible fracture, which is needed for sufficiently piercing the skin.

The folding endurance test was carried out to evaluate the strength of the patches, as shown in Table 3. The MNs were successfully folded and unfolded more than 300 times without encountering any damage or cracks, suggesting that all developed MNs were flexible and exhibited adequate mechanical properties.[23,36] A highly acidic or alkaline pH can cause skin irritation, therefore the surface pH of the prepared MNs was determined. The surface pH of all the samples evaluated was in the range of 6.03 ± 0.01 to 6.24 ± 0.09 (Table 3), indicating that no skin irritation due to pH is expected upon their application.[23,37] To determine the quantity of FUR loaded into the MN patches, FUR-loaded MNs were dissolved to release the encapsulated FUR completely, and the amount of drug was measured based on a calibration curve. High encapsulation efficiency was obtained for FUR-MN formulations, where a decrease was noted as the FUR/PLGA ratio decreased. Even so, drug loading content ranged from 19.1 ± 1% for FUR-MN4 to 28.9 ± 1.4% for FUR-MN2 (Table 3).

The uniform mechanical strength of MNs on an array is an essential indicator for uniform channels created in skin. In this study, ten layers of Parafilm® (Thickness of 140 ± 10 μm) were stacked together as a skin simulant for MN insertion to evaluate the mechanical uniformity of the obtained MNs. After the insertion of MNs on a stack of Parafilm® layers by manu-

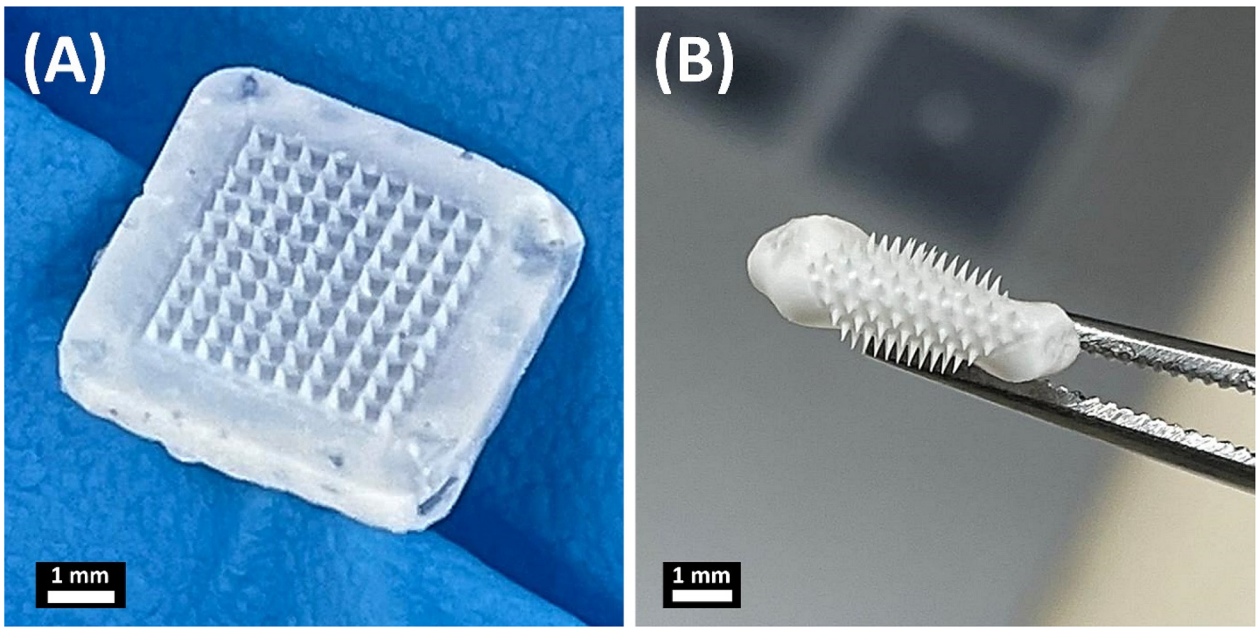

Fig. 2 Representative images of the obtained microneedles: (A) FUR-MN2 and (B) folded FUR-MN2. Scale bar 1 mm.

ally exerted pressure (using a thumb) to simulate the practical use of MNs in clinical settings, each layer was separated and visualized under an optical microscope to measure the dimensions of 10 randomly selected pores. The MNs created about 100% square-shaped pores in the first Parafilm® layer and approximately 80% in the second layer (Fig. 4), in which the length of the square pores was significantly lower than the needle base (Fig. 5). As shown in Fig. 5, the size of the pores decreased from the first to second Parafilm® layer following the pyramidal shape of the MNs. The minimal standard deviation of these demonstrated the uniformity of created pores as well as the mechanical uniformity of the needles. These findings are in agreement with previously published results using pyramidal MNs.[22,24,38]

Previous studies show that manual application of MNs is feasible, reproducible, and may enhance patient compliance by allowing simple self-administration and circumventing the need for an applicator.[25,39] Larrañeta *et al.* report that the measured average forces that patients can apply to polymeric MN arrays were approximately 20 N with no significant difference between male and female volunteers.[25] Other works indicate that the range of forces needed to insert different types of MNs was lower than 20 N.[40–42]

Successful insertion of MNs into skin simulant Parafilm® suggests that MNs easily penetrate the outermost layer of the skin, the *stratum corneum* (~50 μm thickness), consistently and reproducibly by pressing by thumb. This would permit intradermal insertion of the MNs, allowing drug delivery across the skin.[43–45]

MN height reduction for FUR-MNs was evaluated after the insertion test using Parafilm®. Fig. 6 shows the reduction in MN height for all the tested formulations, where the average percent reduction in MN height for FUR-MN2, FUR-MN3 and FUR-MN4 was 10.6%, 9.9% and 7.1%, respectively. These results demonstrate that MNs are mechanically strong and do not fracture, but instead slightly compressed.[46]

Thermal analysis using DSC was performed for PLGA, FUR, FUR-PLGA (1 : 2) physical mixture, and FUR-MN2 (Fig. 7). The DSC thermogram of PLGA shows a glass transition temperature (T_g) at 49.59 °C. The thermogram of FUR is in agreement with the literature:[47,48] It exhibits a melting endotherm at 221.2 °C, followed by an exothermic peak at 224.7 °C, which indicates the crystalline nature of the drug. The peak corresponding to the melting point of FUR in FUR-MN2 is less defined and broader indicating a decrease in the crystallinity of FUR in the MNs.[49] This could be ascribed to a partial drug amorphization occurred during solidification within the PLGA matrix or a thermally-induced amorphization of the system during DSC experiments, as previously reported.[11,50,51]

The PXRD patterns of FUR alone and loaded into PLGA MNs are depicted in Fig. 8. The presence of numerous distinct peaks in both samples indicates that FUR is present in its crystalline form with major characteristic diffraction peaks appearing at a diffraction angle of 2θ (*i.e.*, at 6.02°, 12.05°, 18.12°, 18.96°, 20.49°, 21.35°, 22.91° and 24.79°). Nevertheless, in the case of the FUR-MN2, the intensity of the peaks was reduced. This, together with the less intense melting peak observed in the DSC experiment, indicates a degree of amorphization of the drug within the PLGA matrix.[11,52] The absence of distinct peaks in the XRD pattern for PLGA confirmed its amorphous nature (Fig. S3†).

ATR-FTIR spectra of PLGA, FUR and FUR-MN2 were measured (Fig. 9). Characteristic peaks of FUR at 3400 cm^{-1}, 3282 cm^{-1}, 1670 cm^{-1}, and 1562 cm^{-1} were previously

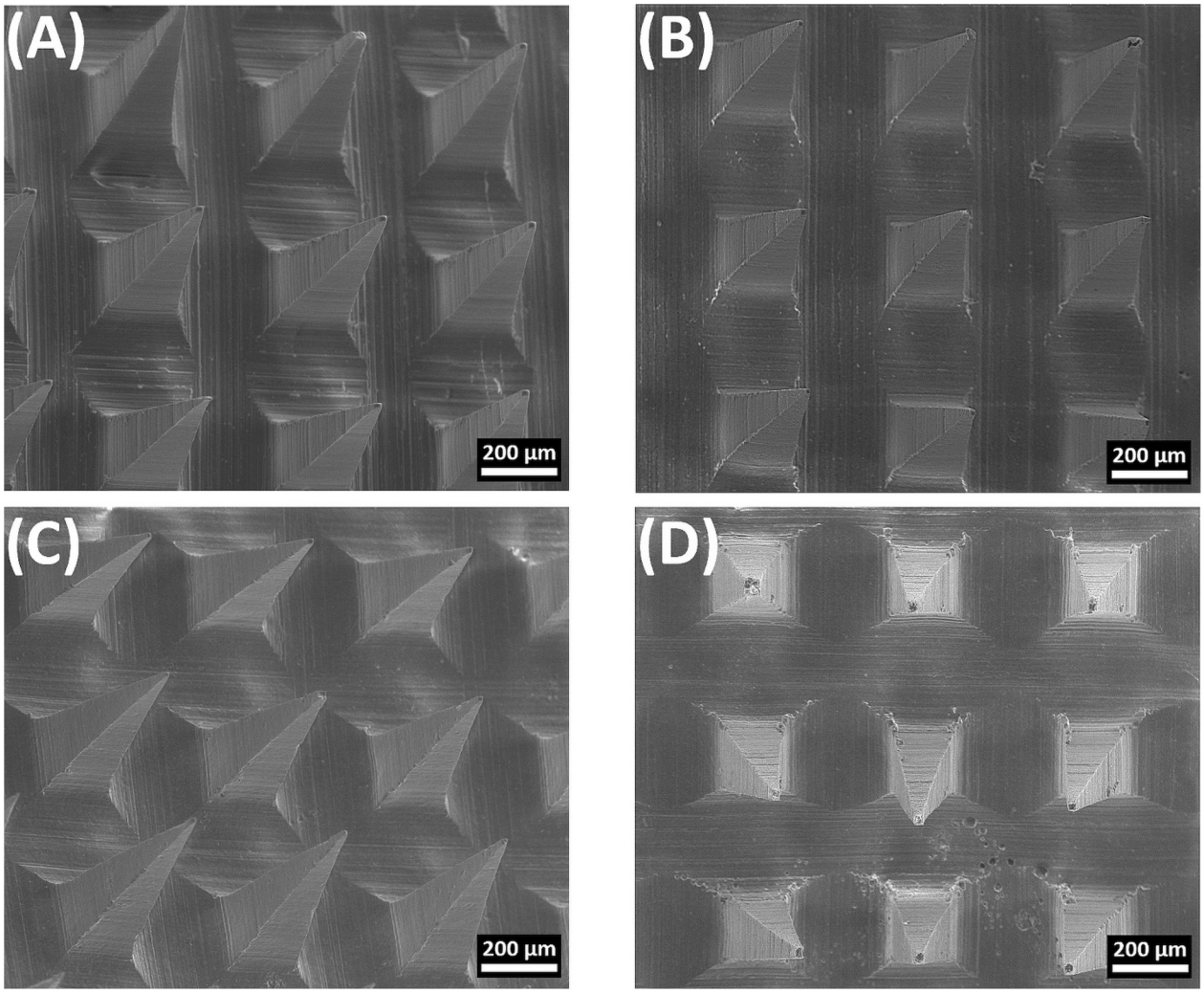

Fig. 3 Representative SEM images of the obtained microneedles: (A) P-MN, (B) FUR-MN2, (C) FUR-MN3, and (D) FUR-MN4. Scale bar 200 μm.

Table 2 Summary of microneedle dimensions (n = 10, mean ± s.d.)

Formulation	Base (μm)	Height (μm)
P-MN	198.76 ± 3.81	494.35 ± 13.46
FUR-MN2	199.31 ± 3.50	499.21 ± 13.78
FUR-MN3	197.65 ± 3.18	496.78 ± 10.92
FUR-MN4	196.62 ± 3.88	497.59 ± 11.60

Table 3 Encapsulation efficiency, drug loading content, surface pH and folding endurance of FUR-MN formulations (n = 3, mean ± s.d.)

	Encapsulation efficiency[a] (%)	Drug loading content[b] (%)	Surface pH	Folding endurance (folds)
FUR-MN2	81.5 ± 5.8	28.9 ± 1.4	6.03 ± 0.01	>300
FUR-MN3	91.5 ± 4.6	23.4 ± 0.9	6.09 ± 0.01	>300
FUR-MN4	94.2 ± 6.1	19.1 ± 1.0	6.24 ± 0.09	>300

[a] Encapsulation efficiency (%) = (amount of drug in MN/amount of drug fed initially) × 100. [b] Drug loading content (%) = [amount of drug/(amount of drug + amount of PLGA)] × 100.

reported.[53,54] The 3400 cm^{-1} band shows the NH_2 stretching vibration of the aromatic ring, and the 3282 cm^{-1} band shows the SO_2NH_2 stretching vibration, while the 1670 cm^{-1} band shows the bending vibration of the amine group. The 1562 cm^{-1} band is assigned to the asymmetric stretching vibration of the carbonyl group. The characteristic peak of PLGA has been reported at 1748 cm^{-1} due to the ester group.

Fig. 9 shows the spectra of FUR, PLGA and FUR-MN2 in which the abovementioned characteristic peaks are evident. There is no significant difference that would indicate chemical interaction between the drug and the PLGA. Differences of 1.2 cm^{-1} and 1.6 cm^{-1} at 3400 and 1670, respectively, maybe ascribed the hydrogen bonding or dipolar interactions.[55,56]

To evaluate the potential application of FUR-loaded MNs, *in vitro* release of FUR from FUR-MN2, FUR-MN3 and FUR-MN4 was tested in PBS pH 7.4 at 37 °C, where sink conditions were maintained. FUR release from MNs exhibits an initial burst release accompanied by a sustained release phase

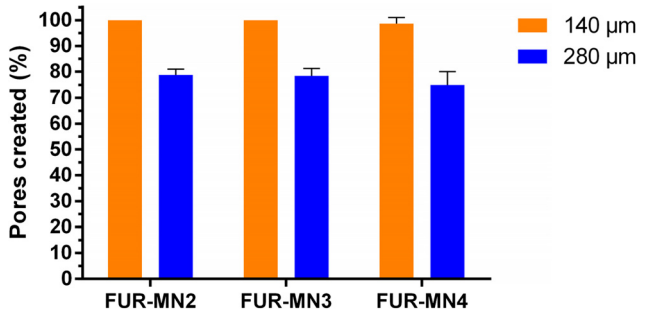

Fig. 4 Insertion test in the Parafilm® skin simulant model: Percentage of MNs that penetrated the first two Parafilm® layers (140 μm and 280 μm depth, respectively) by FUR-MNs, results expressed as means ± s.d., n = 3.

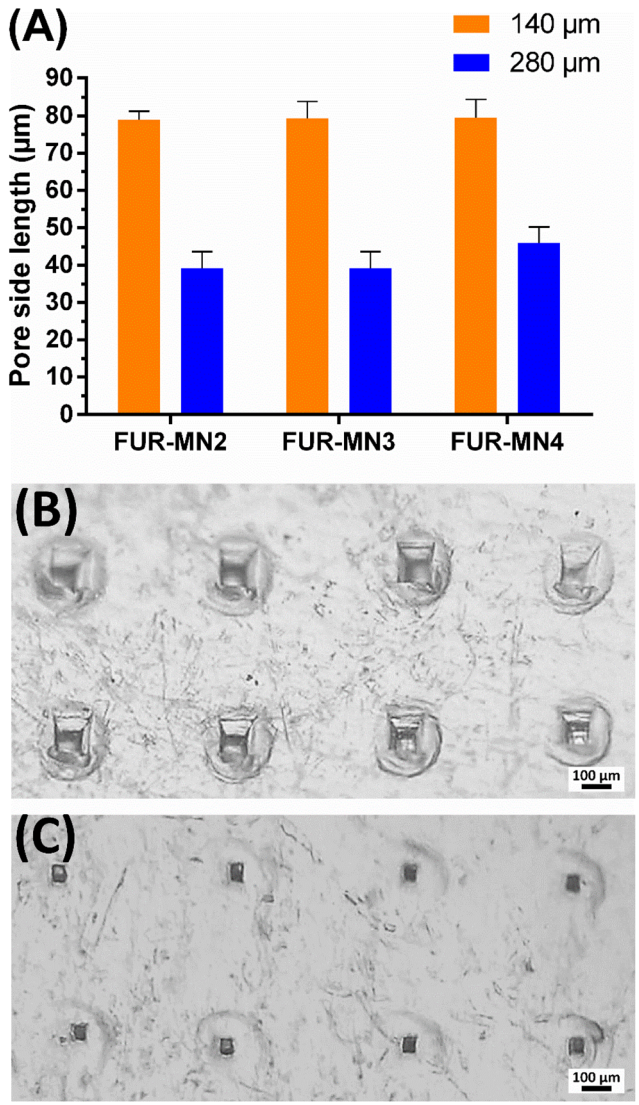

Fig. 5 Insertion test in the Parafilm® skin simulant model. (A) The side length of the pores created by MNs on the first two Parafilm® layers (n = 10, mean ± s.d.). Representative microscopic images of Parafilm® into which FUR-MN2 was inserted: (B) first layer (140 μm), (C) second layer (280 μm). Scale bar 100 μm.

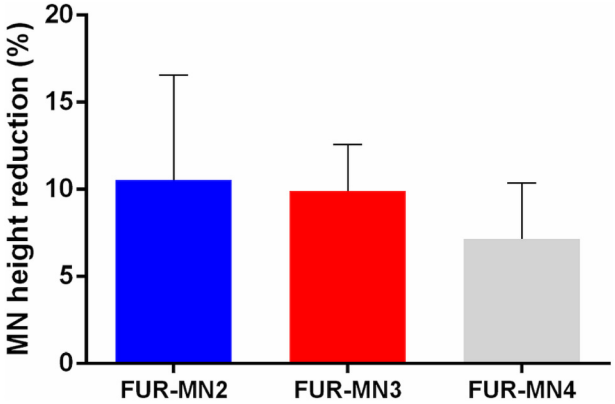

Fig. 6 MN height reduction for MNs after insertion test using the Parafilm® skin simulant model, results expressed as means ± s.d., n = 10.

(Fig. 10). The initial burst release of FUR from MNs is from drug that is weakly bound or adsorbed to the surface.[57] The drug release rate increased by incorporating higher initial drug loading. This observation can be attributed to the effect of the drug load on the polymer matrix itself: the smaller relative amount of polymer due to increased drug load may weaken the function of the network as a physical barrier for drug diffusion. In addition, when drug molecules incorporated into the surface of the polymer matrix dissolve into the release medium, they leave pores *via* which medium can enter the polymer network and facilitate further drug release.[56,58]

The data obtained from *in vitro* release studies were fit to zero-order, first-order and Korsmeyer–Peppas release kinetics models in an attempt to elucidate the release mechanism. The correlation coefficient (R^2) values for the kinetic models are displayed in Table 4, showing that the data best fit first-order release and Korsmeyer–Peppas model.

Our data best fit a first-order kinetic release model, which depicts a release rate that changes proportionally to the concentration of a drug in the donor formulation (*i.e.*, concentration of drug in the MNs). This is often the model that describes release from a drug in matrix diffusion-controlled release. To further understand the dissolution mechanism from the polymer matrix, the data were fit to a Korsmeyer–Peppas model. The obtained release exponents were $0.45 < n < 0.89$, suggesting that drug release follows anomalous non-Fickian transport from the polymer matrix.[59] The release exponent value of FUR-MN2 and FUR-MN3 was approximately 0.5 implying that FUR release is mainly governed by drug diffusion, while FUR-MN4 exhibited a higher n value (n = 0.801) indicating that the drug release was driven by diffusion and partial relaxation of the polymer.[56] A swelling test was performed for FUR-MN2 over 48 h, the duration of the release experiment. After initial slight swelling and relaxation, the swelling ratio remained constant for the last 42 h and no weight loss was measured. This indicates that the release mechanism is controlled mainly by diffusion with only minor contributions from matrix relaxation, degradation, erosion or

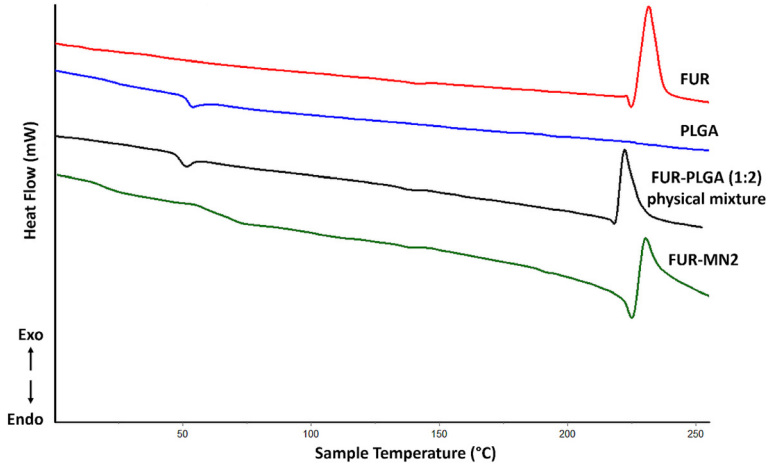

Fig. 7 DSC thermograms of FUR, PLGA, FUR-PLGA (1 : 2) physical mixture, and FUR-MN2.

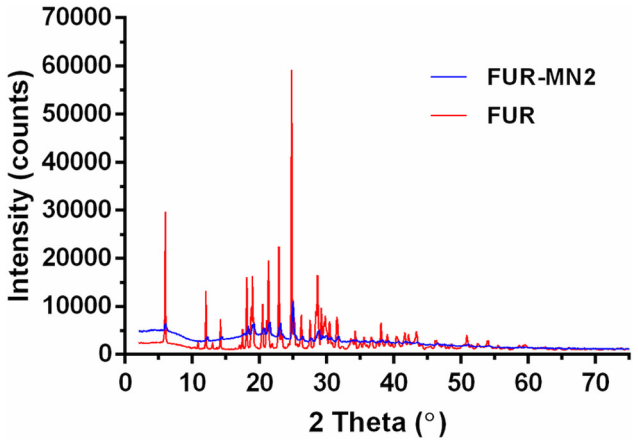

Fig. 8 PXRD of FUR and FUR-MN2.

swelling. This is corroborated by the obtained release exponents (Table 4) which are at the edges of the range of non-Fickian values. The unusual geometry of the MNs may also be responsible for non-Fickian drug release since the mathematical model used was not specifically designed for these unusual geometries and there may be specific physicochemical processes that have not been considered in the model.[60,61]

To further shed light on the mechanical strength of the formulation with the highest drug loading, FUR-MN2, a compression test was carried out using a flat block of aluminum and *ex vivo* chicken skin as counterfaces. Every FUR-MN2 patch tested by compression contained 100 needles and the applied vertical force was normalized by the number of needles (force per a single needle) in the force-displacement curves.

The force-displacement curve of the skin penetration process is shown in Fig. 11A. Three stages were observed in this mechanical strength test: At first, the MNs contacted the skin and the base of the MNs was compressed resulting in a rise on force as displacement increased; Then, the needles were compressed and the force increased until skin penetration, where the inflection point of the force-displacement curve was recorded. After the needles pierced the skin, the force increased sharply. This shows that the MNs penetrated

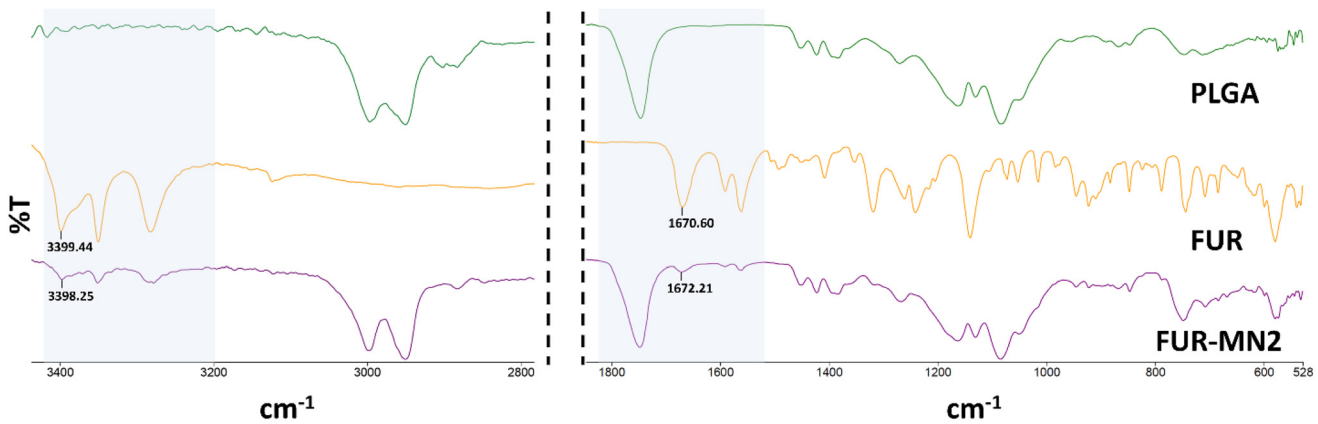

Fig. 9 ATR-FTIR spectra of PLGA, FUR and FUR-MN2.

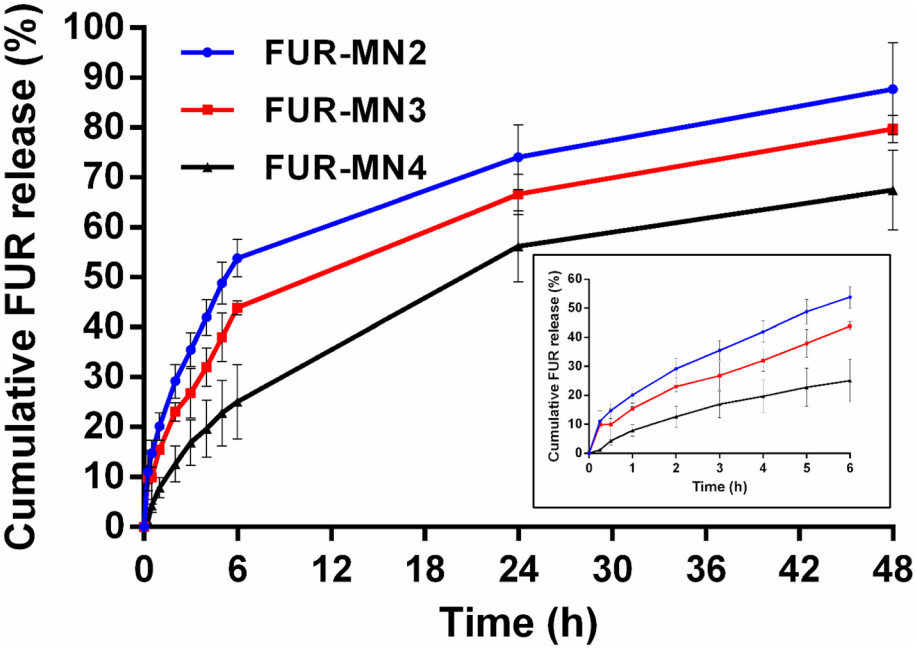

Fig. 10 *In vitro* drug release from microneedles containing varying concentrations of FUR (pH 7.4, 37 °C). Inset shows the drug release profile over the initial 6 h. Values are mean ± s.d. of four experiments.

Table 4 Correlation coefficient (R^2) values of various release kinetic models for microneedles containing varying concentrations of FUR showing the better fit for first order kinetics and giving the release exponent value, *n*, by the Korsmeyer–Peppas model

Formulation	Zero order R^2	First order R^2	Korsmeyer–Peppas model	
			n	R^2
FUR-MN2	0.717	0.930	0.502	0.996
FUR-MN3	0.788	0.934	0.496	0.969
FUR-MN4	0.877	0.949	0.801	0.946

skin.[62] Similar mechanical behavior was reported by Lim *et al.* for PLGA MNs with comparable dimensions during insertion into porcine skin.[63]

Fig. 11B shows the force-displacement curve of the MNs compressed against a flat block of aluminum counterface. The aluminum block is considered to be "completely rigid" relative to the MNs, such that penetration is assumed not to occur. The initial slope of the curve describes the stiffness of the MNs, while the plateau indicates the accelerated deformation process, assumed to be combined buckling and compression, of the MNs due to the absence of penetration into the hard counterface. The elevated value for the plateaus obtained with skin (Fig. 11A) *versus* aluminum (Fig. 11B) clearly indicates that penetration occurs in the case of the skin. As seen in Fig. S4,† MNs show reduction and deformation in the vertical direction but no fracture after compression with the maximum force applied (0.32 N per needle). The average percent reduction in FUR-MN2 height after compression tests on chicken skin and aluminum block was 5.80 ± 2.98% and 11.40 ± 1.70%, respectively (Fig. 11C).

Many efforts have concentrated on attempts to improve FUR performance by enhancing its solubility, absorption and subsequent bioavailability following oral administration.[64–66] Transdermal application of FUR as an alternative route of administration was examined in cats, however, the drug absorption from transdermal administration was negligible compared to that after oral and i.v. administration, due to undetectable drug plasma concentrations at most time points.[67] Interestingly, only few studies have investigated transdermal delivery of FUR, in which penetration enhancers were used to increase the permeation of drug through the *stratum corneum* of the skin.[68–70] To the best of our knowledge, there is only one study reported in the literature about developing FUR-loaded biodegradable polymer MNs, made of poly-ε-caprolactone (PCL) with different MN geometry:[71] MNs containing 20% w/w of FUR (0.77 mg) were fabricated by hot embossing, and the mechanical strength and penetration of the MNs were evaluated using 10% w/w gelatin gel as a counterface, and the drug released completely within 18 h.

Recently, we have seen substantial attempts for reshaping heart management, mainly toward effective and safe out-hospital care. In a phase-II trial, Gilotra *et al.* found no differences in efficacy and safety between i.v. FUR (mean dose: 123 ± 47 mg) and a fixed s.c. dose of 80 mg of pH-neutral FUR formulation when given to patients with acute CHF exacerbation in an out-patient setting. The efficacy of s.c. FUR was demonstrated beyond any doubt by significantly higher 6-hour urine output and more enhanced natriuresis compared to i.v. FUR.[15]

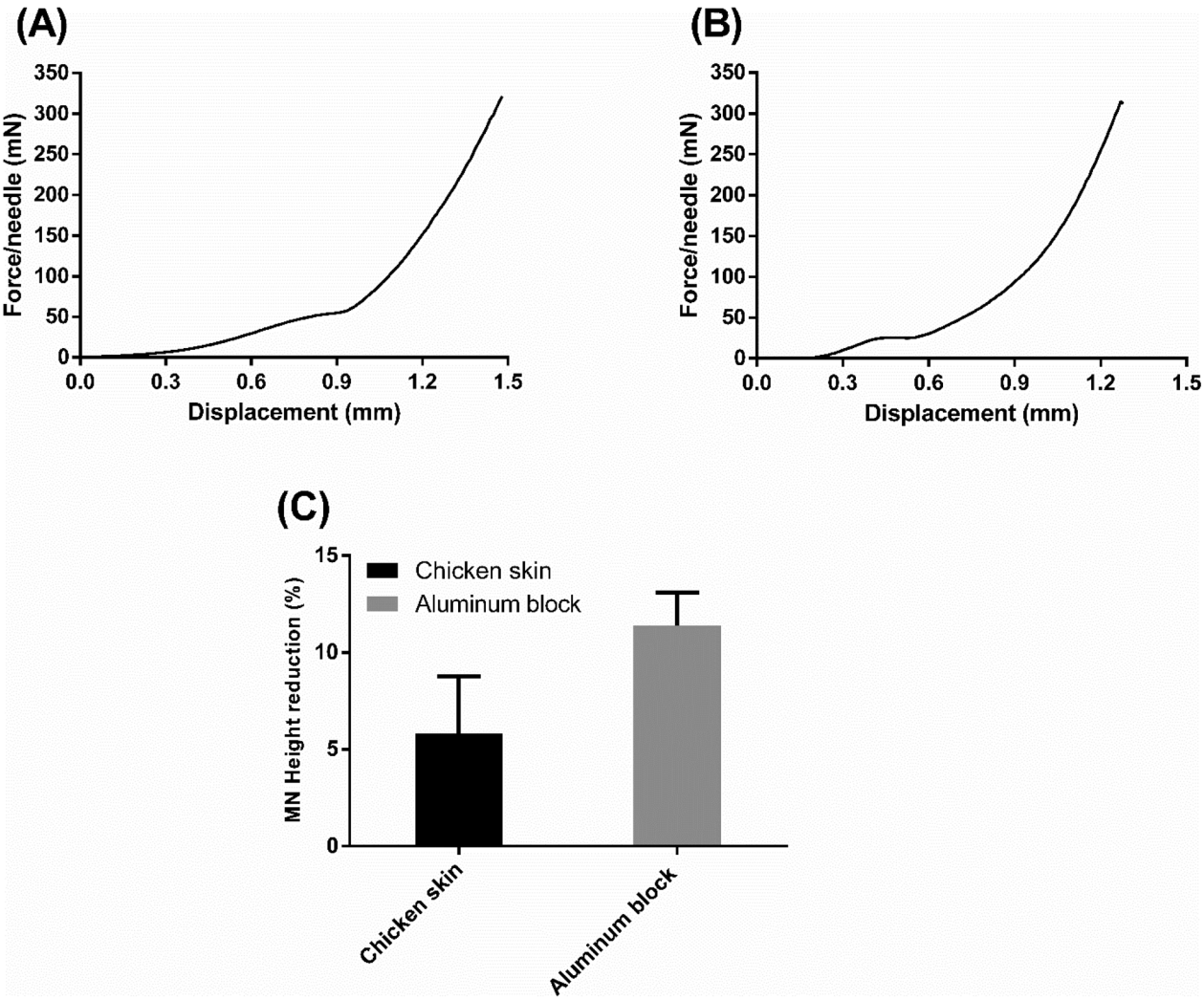

Fig. 11 Microneedle compression tests. (A) Representative force-displacement curve of FUR-MN2 pressed against chicken skin. (B) Representative force-displacement curve of FUR-MN2 pressed against a flat block of aluminum. (C) MN height reduction for MNs after compression tests using the different counterfaces, results expressed as means ± s.d., n = 10.

Yet, this strategy still requires skin canulation when using a syringe pump system in an out-patient setting. In the last decade, intradermal (i.d.) drug delivery has gained interest as an alternative route of drug delivery with enhanced pharmacokinetics. Accordingly, i.d. insulin administration, compared to s.c., increases drug C_{max} (maximal plasma concertation) and decreases T_{max} (the time to maximum plasma concentration), which indicates better post-prandial glycemic control.[20]

This suggests that i.d. FUR delivery using dissolvable MNs patch may be an ideal alternative in various clinical scenarios of CHF, such as early introduction of FUR-MNs patch as soon as the patient becomes stable following i.v. FUR, thereby assuring continuity of sustained and effective diuresis as an alternative to extended i.v. administration. This decreases the risk of peripheral venous catheters, associated with adverse events, and allows early mobility and discharge. An advanced CHF patient, already under high doses of oral FUR, can benefit from FUR MN-patches on a regular basis instead of an alternate i.v. regimen, which would include once or twice a week i.v. FUR therapy. This, again, eliminates the risk adverse events associated with skin canulation and decreases the logistic burden of i.v. home therapy, while ensuring sustained and effective diuresis.

4. Conclusions

To the best of our knowledge, this is the first study to demonstrate the feasibility of fabrication of FUR-loaded biodegradable PLGA MNs as a part of a flexible patch for i.d. delivery. Our results illustrate the fulfillment of chemical and mechanical properties for the desirable self-applicable FUR-MN patch. Further *in vivo* studies are needed to evaluate this novel approach and possibly to expand upon the exciting potential of efficient and safe i.d. delivery of FUR in CHF patients.

Author contributions

Arsalan Abu-Much: Conceptualization, writing – original draft. Raya Darawshi: investigation, methodology, data curation. Hala Dawud: investigation. Haytam Kasem: methodology, writing – review & editing. Aiman Abu Ammar: conceptualization, supervision, methodology, resources, project administration, visualization, formal analysis, funding acquisition, writing – original draft, writing – review & editing.

Conflicts of interest

The authors declare no conflict of interests.

Acknowledgements

The authors would like to acknowledge Rayan Alyan and Israel Dvir for technical support and especially Prof. Deborah Shalev for useful discussions and for reviewing the manuscript. A. Abu Ammar thanks the Azrieli College of Engineering Jerusalem for funding this research.

References

1 M. Azmana, S. Mahmood, A. R. Hilles, U. K. Mandal, K. A. Saeed Al-Japairai and S. Raman, Transdermal Drug Delivery System through Polymeric Microneedle: A Recent Update, *J. Drug Delivery Sci. Technol.*, 2020, **60**, 101877, DOI: 10.1016/j.jddst.2020.101877.

2 L. K. Vora, K. Moffatt, I. A. Tekko, A. J. Paredes, F. Volpe-Zanutto, D. Mishra, K. Peng, T. R. Singh and R. F. Donnelly, Microneedle Array Systems for Long-Acting Drug Delivery, *Eur. J. Pharm. Biopharm.*, 2021, **159**, 44–76, DOI: 10.1016/j.ejpb.2020.12.006.

3 P. R. Yadav, M. N. Munni, L. Campbell, G. Mostofa, L. Dobson, M. Shittu, S. K. Pattanayek, M. J. Uddin and D. B. Das, Translation of Polymeric Microneedles for Treatment of Human Diseases: Recent Trends, Progress, and Challenges, *Pharmaceutics*, 2021, **13**(8), 1132, DOI: 10.3390/pharmaceutics13081132.

4 J. Far, M. Abdel-Haq, M. Gruber and A. Abu Ammar, Developing Biodegradable Nanoparticles Loaded with Mometasone Furoate for Potential Nasal Drug Delivery, *ACS Omega*, 2020, **5**(13), 7432–7439, DOI: 10.1021/acsomega.0c00111.

5 M. Abdel-Haq, R. Alyan, K. Abd-Rbo, H. Kasem and A. Abu Ammar, Biomimetic Clotrimazole-Loaded PLGA Films with Enhanced Adhesiveness for Controlled Drug Release, *Int. J. Pharm.*, 2021, **601**, 120578, DOI: 10.1016/j.ijpharm.2021.120578.

6 A. Abu Ammar, M. Gruber, P. Martin, O. Stern, F. Jahshan, O. Ertracht, E. Sela, S. Srouji and E. Zussman, Local Delivery of Mometasone Furoate from an Eluting Endotracheal Tube, *J. Controlled Release*, 2018, **272**, 54–61, DOI: 10.1016/j.jconrel.2018.01.005.

7 A. Kabha, A. Bukchin-Tihomirov, I. Shlomi, A. Abu Ammar, M. Bidder, G. Amiel and E. Zussman, Biodegradable Controlled-Release Device for Localized Chemotherapeutic Treatment of Bladder Cancer, *ACS Biomater. Sci. Eng.*, 2021, **7**(6), 2548–2557, DOI: 10.1021/acsbiomaterials.1c00339.

8 A. Abu Ammar, A. Nasereddin, S. Ereqat, M. Dan-Goor, C. L. Jaffe, E. Zussman and Z. Abdeen, Amphotericin B-Loaded Nanoparticles for Local Treatment of Cutaneous Leishmaniasis, *Drug Deliv. Transl. Res.*, 2019, **9**(1), 76–84, DOI: 10.1007/s13346-018-00603-0.

9 F. Ruggiero, R. Vecchione, S. Bhowmick, G. Coppola, S. Coppola, E. Esposito, V. Lettera, P. Ferraro and P. A. Netti, Electro-Drawn Polymer Microneedle Arrays with Controlled Shape and Dimension, *Sens. Actuators, B*, 2018, **255**, 1553–1560, DOI: 10.1016/j.snb.2017.08.165.

10 M. He, G. Yang, X. Zhao, S. Zhang and Y. Gao, Intradermal Implantable PLGA Microneedles for Etonogestrel Sustained Release, *J. Pharm. Sci.*, 2020, **109**(6), 1958–1966, DOI: 10.1016/j.xphs.2020.02.009.

11 A. J. Paredes, F. Volpe-Zanutto, A. D. Permana, A. J. Murphy, C. J. Picco, L. K. Vora, J. A. Coulter and R. F. Donnelly, Novel Tip-Loaded Dissolving and Implantable Microneedle Array Patches for Sustained Release of Finasteride, *Int. J. Pharm.*, 2021, **606**, 120885, DOI: 10.1016/j.ijpharm.2021.120885.

12 X. Zhao, S. Zhang, G. Yang, Z. Zhou and Y. Gao, Exploring Trehalose on the Release of Levonorgestrel from Implantable PLGA Microneedles, *Polymers*, 2020, **12**(1), 59, DOI: 10.3390/polym12010059.

13 P. A. Heidenreich, N. M. Albert, L. A. Allen, D. A. Bluemke, J. Butler, G. C. Fonarow, J. S. Ikonomidis, O. Khavjou, M. A. Konstam, T. M. Maddox, G. Nichol, M. Pham, I. L. Piña and J. G. Trogdon, Forecasting the Impact of Heart Failure in the United States: A Policy Statement From the American Heart Association, *Circ.: Heart Failure*, 2013, **6**(3), 606–619, DOI: 10.1161/HHF.0b013e318291329a.

14 T. A. McDonagh, M. Metra, M. Adamo, R. S. Gardner, A. Baumbach, M. Böhm, H. Burri, J. Butler, J. Čelutkienė, O. Chioncel, J. G. F. Cleland, A. J. S. Coats, M. G. Crespo-Leiro, D. Farmakis, M. Gilard, S. Heymans, A. W. Hoes, T. Jaarsma, E. A. Jankowska, M. Lainscak, C. S. P. Lam, A. R. Lyon, J. J. V. McMurray, A. Mebazaa, R. Mindham, C. Muneretto, M. Francesco Piepoli, S. Price, G. M. C. Rosano, F. Ruschitzka, A. Kathrine Skibelund, ESC Scientific Document Group, R. A. de Boer, P. Christian Schulze, M. Abdelhamid, V. Aboyans, S. Adamopoulos, S. D. Anker, E. Arbelo, R. Asteggiano, J. Bauersachs, A. Bayes-Genis, M. A. Borger, W. Budts, M. Cikes, K. Damman, V. Delgado, P. Dendale, P. Dilaveris, H. Drexel, J. Ezekowitz, V. Falk, L. Fauchier, G. Filippatos, A. Fraser, N. Frey, C. P. Gale, F. Gustafsson, J. Harris, B. Iung, S. Janssens, M. Jessup, A. Konradi, D. Kotecha, E. Lambrinou, P. Lancellotti, U. Landmesser, C. Leclercq, B. S. Lewis, F. Leyva, A. Linhart, M.-L. Løchen, L. H. Lund,

D. Mancini, J. Masip, D. Milicic, C. Mueller, H. Nef, J.-C. Nielsen, L. Neubeck, M. Noutsias, S. E. Petersen, A. Sonia Petronio, P. Ponikowski, E. Prescott, A. Rakisheva, D. J. Richter, E. Schlyakhto, P. Seferovic, M. Senni, M. Sitges, M. Sousa-Uva, C. G. Tocchetti, R. M. Touyz, C. Tschoepe, J. Waltenberger, M. Adamo, A. Baumbach, M. Böhm, H. Burri, J. Čelutkienė, O. Chioncel, J. G. F. Cleland, A. J. S. Coats, M. G. Crespo-Leiro, D. Farmakis, R. S. Gardner, M. Gilard, S. Heymans, A. W. Hoes, T. Jaarsma, E. A. Jankowska, M. Lainscak, C. S. P. Lam, A. R. Lyon, J. J. V. McMurray, A. Mebazaa, R. Mindham, C. Muneretto, M. F. Piepoli, S. Price, G. M. C. Rosano, F. Ruschitzka and A. K. Skibelund, 2021 ESC Guidelines for the Diagnosis and Treatment of Acute and Chronic Heart Failure, *Eur. Heart J.*, 2021, **42**(36), 3599–3726, DOI: **10.1093/eurheartj/ehab368**.

15 N. A. Gilotra, O. Princewill, B. Marino, I. S. Okwuosa, J. Chasler, J. Almansa, A. Cummings, P. Rhodes, J. Chambers, K. Cuomo and S. D. Russell, Efficacy of Intravenous Furosemide Versus a Novel, PH-Neutral Furosemide Formulation Administered Subcutaneously in Outpatients With Worsening Heart Failure, *JACC: Heart Failure*, 2018, **6**(1), 65–70, DOI: **10.1016/j.jchf.2017.10.001**.

16 D. H. Ellison and G. M. Felker, Diuretic Treatment in Heart Failure, *N. Engl. J. Med.*, 2017, **377**(20), 1964–1975, DOI: **10.1056/NEJMra1703100**.

17 K. Miliani, R. Taravella, D. Thillard, V. Chauvin, E. Martin, S. Edouard, P. Astagneau and CATHEVAL Study Group, Peripheral Venous Catheter-Related Adverse Events: Evaluation from a Multicentre Epidemiological Study in France (the CATHEVAL Project), *PLoS One*, 2017, **12**(1), e0168637, DOI: **10.1371/journal.pone.0168637**.

18 D. A. Sica, P. Muntendam, R. L. Myers, J. M. ter Maaten, M. E. Sale, R. A. de Boer and B. Pitt, Subcutaneous Furosemide in Heart Failure, *JACC: Basic Transl. Sci.*, 2018, **3**(1), 25–34, DOI: **10.1016/j.jacbts.2017.10.001**.

19 J. Civera, R. de la Espriella, R. Heredia, G. Miñana, E. Santas, A. Conesa, A. Mollar, C. Sastre, A. Martínez, A. Villaescusa and J. Núñez, Efficacy and Safety of Subcutaneous Infusion of Non-Formulated Furosemide in Patients with Worsening Heart Failure: A Real-World Study, *J. Cardiovasc. Transl. Res.*, 2022, **15**, 644–652.

20 R. J. Pettis, L. Hirsch, C. Kapitza, L. Nosek, U. Hövelmann, H.-J. Kurth, D. E. Sutter, N. G. Harvey and L. Heinemann, Microneedle-Based Intradermal Versus Subcutaneous Administration of Regular Human Insulin or Insulin Lispro: Pharmacokinetics and Postprandial Glycemic Excursions in Patients with Type 1 Diabetes, *Diabetes Technol. Ther.*, 2011, **13**(4), 443–450, DOI: **10.1089/dia.2010.0183**.

21 J. Jacobse, W. Voorde, A. Tandon, S. G. Romeijn, H. W. Grievink, K. Maaden, M. J. Esdonk, D. J. A. R. Moes, F. Loeff, K. Bloem, A. Vries, T. Rispens, G. Wolbink, M. Kam, D. Ziagkos, M. Moerland, W. Jiskoot, J. Bouwstra, J. Burggraaf, L. Schrier, R. Rissmann and R. Cate, Comprehensive Evaluation of Microneedle–based Intradermal Adalimumab Delivery *vs.* Subcutaneous Administration: Results of a Randomized Controlled Clinical Trial, *Br. J. Clin. Pharmacol.*, 2021, **87**(8), 3162–3176, DOI: **10.1111/bcp.14729**.

22 M. S. Arshad, S. Fatima, K. Nazari, R. Ali, M. Farhan, S. A. Muhammad, N. Abbas, A. Hussain, I. Kucuk, M.-W. Chang, P. Mehta and Z. Ahmad, Engineering and Characterisation of BCG-Loaded Polymeric Microneedles, *J. Drug Targeting*, 2020, **28**(5), 525–532, DOI: **10.1080/1061186X.2019.1693577**.

23 P. W. R. Ananda, D. Elim, H. S. Zaman, W. Muslimin, M. G. R. Tunggeng and A. D. Permana, Combination of Transdermal Patches and Solid Microneedles for Improved Transdermal Delivery of Primaquine, *Int. J. Pharm.*, 2021, **609**, 121204, DOI: **10.1016/j.ijpharm.2021.121204**.

24 H. X. Nguyen, B. D. Bozorg, Y. Kim, A. Wieber, G. Birk, D. Lubda and A. K. Banga, Poly (Vinyl Alcohol) Microneedles: Fabrication, Characterization, and Application for Transdermal Drug Delivery of Doxorubicin, *Eur. J. Pharm. Biopharm.*, 2018, **129**, 88–103, DOI: **10.1016/j.ejpb.2018.05.017**.

25 E. Larrañeta, J. Moore, E. M. Vicente-Pérez, P. González-Vázquez, R. Lutton, A. D. Woolfson and R. F. Donnelly, A Proposed Model Membrane and Test Method for Microneedle Insertion Studies, *Int. J. Pharm.*, 2014, **472**(1–2), 65–73, DOI: **10.1016/j.ijpharm.2014.05.042**.

26 P. Weimer, R. C. Rossi and L. S. Koester, Dissolving Microneedles Developed in Association with Nanosystems: A Scoping Review on the Quality Parameters of These Emerging Systems for Drug or Protein Transdermal Delivery, *Pharmaceutics*, 2021, **13**(10), 1601, DOI: **10.3390/pharmaceutics13101601**.

27 K. Peng, L. K. Vora, I. A. Tekko, A. D. Permana, J. Domínguez-Robles, D. Ramadon, P. Chambers, H. O. McCarthy, E. Larrañeta and R. F. Donnelly, Dissolving Microneedle Patches Loaded with Amphotericin B Microparticles for Localised and Sustained Intradermal Delivery: Potential for Enhanced Treatment of Cutaneous Fungal Infections, *J. Controlled Release*, 2021, **339**, 361–380, DOI: **10.1016/j.jconrel.2021.10.001**.

28 W. Li, J. Tang, R. N. Terry, S. Li, A. Brunie, R. L. Callahan, R. K. Noel, C. A. Rodríguez, S. P. Schwendeman and M. R. Prausnitz, Long-Acting Reversible Contraception by Effervescent Microneedle Patch, *Sci. Adv.*, 2019, **5**(11), eaaw8145, DOI: **10.1126/sciadv.aaw8145**.

29 M. Das and P. Senapati, Furosemide-Loaded Alginate Microspheres Prepared by Ionic Cross-Linking Technique: Morphology and Release Characteristics, *Indian J. Pharm. Sci.*, 2008, **70**(1), 77, DOI: **10.4103/0250-474X.40336**.

30 H. Kasem, H. Shriki, L. Ganon, M. Mizrahi, K. Abd-Rbo and A. J. Domb, Rubber Plunger Surface Texturing for Friction Reduction in Medical Syringes, *Friction*, 2019, **7**(4), 351–358, DOI: **10.1007/s40544-018-0227-5**.

31 R. Justin, S. Román, D. Chen, K. Tao, X. Geng, R. T. Grant, S. MacNeil, K. Sun and B. Chen, Biodegradable and Conductive Chitosan–Graphene Quantum Dot

Nanocomposite Microneedles for Delivery of Both Small and Large Molecular Weight Therapeutics, *RSC Adv.*, 2015, **5**(64), 51934–51946, DOI: **10.1039/C5RA04340A**.

32 P. Zhang, C. Dalton and G. A. Jullien, Design and Fabrication of MEMS-Based Microneedle Arrays for Medical Applications, *Microsyst. Technol.*, 2009, **15**(7), 1073–1082, DOI: **10.1007/s00542-009-0883-5**.

33 I. Ramöller, E. McAlister, A. Bogan, A. Cordeiro and R. Donnelly, Novel Design Approaches in the Fabrication of Polymeric Microarray Patches via Micromoulding, *Micromachines*, 2020, **11**(6), 554, DOI: **10.3390/mi11060554**.

34 K. Pamlényi, K. Kristó, O. Jójárt-Laczkovich and G. Regdon, Formulation and Optimization of Sodium Alginate Polymer Film as a Buccal Mucoadhesive Drug Delivery System Containing Cetirizine Dihydrochloride, *Pharmaceutics*, 2021, **13**(5), 619, DOI: **10.3390/pharmaceutics13050619**.

35 K. A. Moga, L. R. Bickford, R. D. Geil, S. S. Dunn, A. A. Pandya, Y. Wang, J. H. Fain, C. F. Archuleta, A. T. O'Neill and J. M. DeSimone, Rapidly-Dissolvable Microneedle Patches Via a Highly Scalable and Reproducible Soft Lithography Approach, *Adv. Mater.*, 2013, **25**(36), 5060–5066, DOI: **10.1002/adma.201300526**.

36 L. Rahman, R. S. Lembang, S. Lallo, S. R. Handayani, U. Usmanengsi and A. D. Permana, Bioadhesive Dermal Patch as Promising Approach for Improved Antibacterial Activity of Bioactive Compound of Zingiber Cassumunar Roxb in Ex Vivo Staphylococcus Aureus Skin Infection Model, *J. Drug Delivery Sci. Technol.*, 2021, **63**, 102522, DOI: **10.1016/j.jddst.2021.102522**.

37 E. A. Almazan, P. S. Castañeda, R. D. Torres and J. J. Escobar-Chavez, Design and Evaluation of Losartan Transdermal Patch by Using Solid Microneedles as A Physical Permeation Enhancer, *Iran J. Pharm. Res.*, 2020, **19**(1), 138–152, DOI: **10.22037/ijpr.2019.1100912**.

38 H. X. Nguyen and A. K. Banga, Fabrication, Characterization and Application of Sugar Microneedles for Transdermal Drug Delivery, *Ther. Delivery*, 2017, **8**(5), 249–264, DOI: **10.4155/tde-2016-0096**.

39 R. F. Donnelly, K. Moffatt, A. Z. Alkilani, E. M. Vicente-Pérez, J. Barry, M. T. C. McCrudden and A. D. Woolfson, Hydrogel-Forming Microneedle Arrays Can Be Effectively Inserted in Skin by Self-Application: A Pilot Study Centred on Pharmacist Intervention and a Patient Information Leaflet, *Pharm. Res.*, 2014, **31**(8), 1989–1999, DOI: **10.1007/s11095-014-1301-y**.

40 S. P. Davis, B. J. Landis, Z. H. Adams, M. G. Allen and M. R. Prausnitz, Insertion of Microneedles into Skin: Measurement and Prediction of Insertion Force and Needle Fracture Force, *J. Biomech.*, 2004, **37**(8), 1155–1163, DOI: **10.1016/j.jbiomech.2003.12.010**.

41 X. Q. Kong, P. Zhou and C. W. Wu, Numerical Simulation of Microneedles' Insertion into Skin, *Comput. Methods Biomech. Biomed. Eng.*, 2011, **14**(9), 827–835, DOI: **10.1080/10255842.2010.497144**.

42 W. W. Koelmans, G. Krishnamoorthy, A. Heskamp, J. Wissink, S. Misra and N. Tas, Microneedle Characterization Using a Double-Layer Skin Simulant, *MER*, 2013, **3**(2), p51, DOI: **10.5539/mer.v3n2p51**.

43 M. S. Arshad, S. Zafar, A. T. Zahra, M. H. Zaman, A. Akhtar, I. Kucuk, M. Farhan, M.-W. Chang and Z. Ahmad, Fabrication and Characterisation of Self-Applicating Heparin Sodium Microneedle Patches, *J. Drug Targeting*, 2021, **29**(1), 60–68, DOI: **10.1080/1061186X.2020.1795180**.

44 A. J. Courtenay, E. McAlister, M. T. C. McCrudden, L. Vora, L. Steiner, G. Levin, E. Levy-Nissenbaum, N. Shterman, M.-C. Kearney, H. O. McCarthy and R. F. Donnelly, Hydrogel-Forming Microneedle Arrays as a Therapeutic Option for Transdermal Esketamine Delivery, *J. Controlled Release*, 2020, **322**, 177–186, DOI: **10.1016/j.jconrel.2020.03.026**.

45 A. H. B. Sabri, Q. K. Anjani and R. F. Donnelly, Synthesis and Characterization of Sorbitol Laced Hydrogel-Forming Microneedles for Therapeutic Drug Monitoring, *Int. J. Pharm.*, 2021, **607**, 121049, DOI: **10.1016/j.ijpharm.2021.121049**.

46 A. A. Albadr, I. A. Tekko, L. K. Vora, A. A. Ali, G. Laverty, R. F. Donnelly and R. R. S. Thakur, Rapidly Dissolving Microneedle Patch of Amphotericin B for Intracorneal Fungal Infections, *Drug Deliv. Transl. Res.*, 2022, **12**(4), 931–943, DOI: **10.1007/s13346-021-01032-2**.

47 M. Vlachou, S. Kikionis, A. Siamidi, S. Kyriakou, A. Tsotinis, E. Ioannou and V. Roussis, Development and Characterization of Eudragit®-Based Electrospun Nanofibrous Mats and Their Formulation into Nanofiber Tablets for the Modified Release of Furosemide, *Pharmaceutics*, 2019, **11**(9), 480, DOI: **10.3390/pharmaceutics11090480**.

48 J. A. Miranda, C. Garnero, A. Zoppi, V. Sterren, A. P. Ayala and M. R. Longhi, Characterization of Systems with Amino-Acids and Oligosaccharides as Modifiers of Biopharmaceutical Properties of Furosemide, *J. Pharm. Biomed. Anal.*, 2018, **149**, 143–150, DOI: **10.1016/j.jpba.2017.10.038**.

49 B. P. Sahu and M. K. Das, Nanoprecipitation with Sonication for Enhancement of Oral Bioavailability of Furosemide, *Acta Pol. Pharm.*, 2014, **71**(1), 129–137.

50 A. J. Paredes, N. M. Camacho, L. Schofs, A. Dib, M. Zarazaga, P. del, N. Litterio, D. A. Allemandi, S. Sánchez Bruni, C. Lanusse and S. D. Palma, Ricobendazole Nanocrystals Obtained by Media Milling and Spray Drying: Pharmacokinetic Comparison with the Micronized Form of the Drug, *Int. J. Pharm.*, 2020, **585**, 119501, DOI: **10.1016/j.ijpharm.2020.119501**.

51 A. Simonazzi, A. G. Cid, A. J. Paredes, L. Schofs, E. E. Gonzo, S. D. Palma and J. M. Bermúdez, Development and in Vitro Evaluation of Solid Dispersions as Strategy to Improve Albendazole Biopharmaceutical Behavior, *Ther. Delivery*, 2018, **9**(9), 623–638, DOI: **10.4155/tde-2018-0037**.

52 R. P. Patel, D. J. Patel, D. B. Bhimani and J. K. Patel, Physicochemical Characterization and Dissolution Study of

Solid Dispersions of Furosemide with Polyethylene Glycol 6000 and Polyvinylpyrrolidone K30, *Dissolution Technol.*, 2008, **15**(3), 17–25, DOI: 10.14227/DT150308P17.

53 I. Youm, J. B. Murowchick and B.-B. C. Youan, Entrapment and Release Kinetics of Furosemide from Pegylated Nanocarriers, *Colloids Surf., B*, 2012, **94**, 133–142, DOI: 10.1016/j.colsurfb.2012.01.027.

54 S. Kashyap, A. Singh, A. Mishra and V. Singh, Enhanced Sustained Release of Furosemide in Long Circulating Chitosan-Conjugated PLGA Nanoparticles, *Results Pharma Sci.*, 2019, **14**(2), 93, DOI: 10.4103/1735-5362.253356.

55 Y. Chen, S. Wang, S. Wang, C. Liu, C. Su, M. Hageman, M. Hussain, R. Haskell, K. Stefanski and F. Qian, Initial Drug Dissolution from Amorphous Solid Dispersions Controlled by Polymer Dissolution and Drug-Polymer Interaction, *Pharm. Res.*, 2016, **33**(10), 2445–2458, DOI: 10.1007/s11095-016-1969-2.

56 E. Utomo, J. Domínguez-Robles, N. Moreno-Castellanos, S. A. Stewart, C. J. Picco, Q. K. Anjani, J. A. Simón, I. Peñuelas, R. F. Donnelly and E. Larrañeta, Development of Intranasal Implantable Devices for Schizophrenia Treatment, *Int. J. Pharm.*, 2022, **624**, 122061, DOI: 10.1016/j.ijpharm.2022.122061.

57 L. L. Lao, S. S. Venkatraman and N. A. Peppas, Modeling of Drug Release from Biodegradable Polymer Blends, *Eur. J. Pharm. Biopharm.*, 2008, **70**(3), 796–803, DOI: 10.1016/j.ejpb.2008.05.024.

58 Y. Xu, C.-S. Kim, D. M. Saylor and D. Koo, Polymer Degradation and Drug Delivery in PLGA-Based Drug-Polymer Applications: A Review of Experiments and Theories: Review On Biodegradation And Drug Delivery From PLGA Polymers, *J. Biomed. Mater. Res.*, 2017, **105**(6), 1692–1716, DOI: 10.1002/jbm.b.33648.

59 S. Dash, P. N. Murthy, L. Nath and P. Chowdhury, Kinetic Modeling on Drug Release from Controlled Drug Delivery Systems, *Acta Pol. Pharm.*, 2010, **67**(3), 217–223.

60 P. L. Ritger and N. A. Peppas, A Simple Equation for Description of Solute Release I. Fickian and Non-Fickian Release from Non-Swellable Devices in the Form of Slabs, Spheres, Cylinders or Discs, *J. Controlled Release*, 1987, **5**(1), 23–36, DOI: 10.1016/0168-3659(87)90034-4.

61 Y. Fu and W. J. Kao, Drug Release Kinetics and Transport Mechanisms of Non-Degradable and Degradable Polymeric Delivery Systems, *Expert Opin. Drug Delivery*, 2010, **7**(4), 429–444, DOI: 10.1517/17425241003602259.

62 Q. Zhang, C. Xu, S. Lin, H. Zhou, G. Yao, H. Liu, L. Wang, X. Pan, G. Quan and C. Wu, Synergistic Immunoreaction of Acupuncture-like Dissolving Microneedles Containing Thymopentin at Acupoints in Immune-Suppressed Rats, *Acta Pharm. Sin. B*, 2018, **8**(3), 449–457, DOI: 10.1016/j.apsb.2017.12.006.

63 H. Lim, S. Ha, M. Bae and S.-H. Yoon, A Highly Robust Approach to Fabricate the Mass-Customizable Mold of Sharp-Tipped Biodegradable Polymer Microneedles for Drug Delivery, *Int. J. Pharm.*, 2021, **600**, 120475, DOI: 10.1016/j.ijpharm.2021.120475.

64 C. J. Van der Merwe, J. D. Steyn, J. H. Hamman, W. Pheiffer, H. Svitina, B. Peterson and J. H. Steenekamp, Effect of Functional Excipients on the Dissolution and Membrane Permeation of Furosemide Formulated into Multiple-Unit Pellet System (MUPS) Tablets, *Pharm. Dev. Technol.*, 2022, **27**(5), 572–587, DOI: 10.1080/10837450.2022.2089898.

65 G. Murtaza, S. A. Khan, M. Najam-ul-Haq and I. Hussain, Comparative Evaluation of Various Solubility Enhancement Strategies for Furosemide, *Pak. J. Pharm. Sci.*, 2014, **27**(4), 963–973.

66 R. Ghadi and N. Dand, BCS Class IV Drugs: Highly Notorious Candidates for Formulation Development, *J. Controlled Release*, 2017, **248**, 71–95, DOI: 10.1016/j.jconrel.2017.01.014.

67 M. M. Sleeper, P. O'Donnell, C. Fitzgerald and M. G. Papich, Pharmacokinetics of Furosemide after Intravenous, Oral and Transdermal Administration to Cats, *J. Feline Med. Surg.*, 2019, **21**(10), 882–886, DOI: 10.1177/1098612X18805879.

68 D. P. Patel, C. M. Setty, G. N. Mistry, S. L. Patel, T. J. Patel, P. C. Mistry, A. K. Rana, P. K. Patel and R. S. Mishra, Development and Evaluation of Ethyl Cellulose-Based Transdermal Films of Furosemide for Improved In Vitro Skin Permeation, *AAPS PharmSciTech*, 2009, **10**(2), 437–442, DOI: 10.1208/s12249-009-9224-3.

69 I.-H. Chang, H.-Y. Cho, J.-H. Noh, J.-C. Park, Y.-S. Park, S.-J. Kim and S.-C. Shin, Enhanced Transdermal Delivery of Furosemide from the EVA Matrix through the Rat Skin, *J. Korean Pharm. Sci.*, 2009, **39**(1), 19–21, DOI: 10.4333/KPS.2009.39.1.019.

70 G. G. Agyralides, P. P. Dallas and D. M. Rekkas, Development and in Vitro Evaluation of Furosemide Transdermal Formulations Using Experimental Design Techniques, *Int. J. Pharm.*, 2004, **281**(1–2), 35–43, DOI: 10.1016/j.ijpharm.2004.05.011.

71 T. E. Andersen, A. J. Andersen, R. S. Petersen, L. H. Nielsen and S. S. Keller, Drug Loaded Biodegradable Polymer Microneedles Fabricated by Hot Embossing, *Microelectron. Eng.*, 2018, **195**, 57–61, DOI: 10.1016/j.mee.2018.03.024.